Title

Chronic intermittent ethanol exposure disrupts stress-related tripartite communication to impact affect-related behavioral selection in male rats

Authors

Munier, JJ
Shen, S
Rahal, D
et al.

Publication Date

2023-05-01

DOI

10.1016/j.ynstr.2023.100539

Peer reviewed

Neurobiology of Stress 24 (2023) 100539

Contents lists available at ScienceDirect

Neurobiology of Stress

journal homepage: www.elsevier.com/locate/ynstr

Chronic intermittent ethanol exposure disrupts stress-related tripartite communication to impact affect-related behavioral selection in male rats

J.J. Munier [a,*], S. Shen [a,1], D. Rahal [b,1], A. Hanna [a], V.N. Marty [a], P.R. O'Neill [c], M.S. Fanselow [d], I. Spigelman [a,**]

[a] Laboratory of Neuropharmacology, Section of Biosystems & Function, School of Dentistry, UCLA, United States
[b] Edna Bennett Pierce Prevention Research Center, The Pennsylvania State University, United States
[c] Hatos Center for Neuropharmacology, Department of Psychiatry & Biobehavioral Sciences, David Geffen School of Medicine, UCLA, United States
[d] Department of Psychology, College of Life Sciences, Department of Psychiatry & Biobehavioral Science, David Geffen School of Medicine, UCLA, United States

ARTICLE INFO

Handling Editor: Rita Valentino

ABSTRACT

Alcohol use disorder (AUD) is characterized by loss of intake control, increased anxiety, and susceptibility to relapse inducing stressors. Both astrocytes and neurons contribute to behavioral and hormonal consequences of chronic intermittent ethanol (CIE) exposure in animal models. Details on how CIE disrupts hypothalamic neuro-glial communication, which mediates stress responses are lacking. We conducted a behavioral battery (grooming, open field, reactivity to a single, uncued foot-shock, intermittent-access two-bottle choice ethanol drinking) followed by Ca^{2+} imaging in *ex-vivo* slices of paraventricular nucleus of the hypothalamus (PVN) from male rats exposed to CIE vapor or air-exposed controls. Ca^{2+} signals were evaluated in response to norepinephrine (NE) with or without selective α-adrenergic receptor (αAR) or GluN2B-containing N-methyl-D-aspartate receptor (NMDAR) antagonists, followed by dexamethasone (DEX) to mock a pharmacological stress response. Expectedly, CIE rats had altered anxiety-like, rearing, grooming, and drinking behaviors. Importantly, NE-mediated reductions in Ca^{2+} event frequency were blunted in both CIE neurons and astrocytes. Administration of the selective α1AR antagonist, prazosin, reversed this CIE-induced dysfunction in both cell types. Additionally, the pharmacological stress protocol reversed the altered basal Ca^{2+} signaling profile of CIE astrocytes. Signaling changes in astrocytes in response to NE were correlated with anxiety-like behaviors, such as the grooming: rearing ratio, suggesting tripartite synaptic function plays a role in switching between exploratory and stress-coping behavior. These data show how CIE exposure causes persistent changes to PVN neuro-glial function and provides the groundwork for how these physiological changes manifest in behavioral selection.

1. Introduction

Alcohol misuse is a persistent global health concern that is associated with societal and financial costs exceeding $249 billion per year (Peltier et al., 2019; Sacks et al., 2015). Attempts to pharmacologically treat AUD are hindered by both reluctance to seek treatment (Blanco et al., 2015) and interindividual differences in the underlying mechanisms (Heilig et al., 2016; Wilcox et al., 2018). Establishment of behavioral biomarkers as predictors of pharmacological efficacy can help clinicians understand the underlying mechanisms that contribute to variance in drug treatments and provide improved personalized treatment plans (Heilig et al., 2016).

The hypothalamic-pituitary-adrenal (HPA) axis is a coordinated neuroendocrine system that allows the host to adaptively respond to threatening stimuli (Smith and Vale, 2006). This axis is initiated through the activation of parvocellular neurosecretory cells (PNCs) containing corticotropin-releasing factor (CRF) within the paraventricular nucleus of the hypothalamus (PVN) by glutamatergic and noradrenergic inputs. Ultimately, HPA axis activation results in the release of cortisol (CORT) from the adrenal cortex that negatively regulates the activity of these

* Corresponding author.
** Corresponding author. Laboratory of Neuropharmacology, Section of Biosystems & Function, School of Dentistry, UCLA, 10833 Le Conte Avenue, 63-078 CHS, Los Angeles, CA, 90095-1668, United States.
E-mail addresses: jmunier@ucla.edu (J.J. Munier), ispigelman@dentistry.ucla.edu (I. Spigelman).
[1] Indicates equal author contributions.

https://doi.org/10.1016/j.ynstr.2023.100539
Received 22 November 2022; Received in revised form 12 April 2023; Accepted 16 April 2023
Available online 20 April 2023

CRF cells (Smith and Vale, 2006). Additionally, CRF cells must coordinate upstream afferent signals from the locus coeruleus and amygdala (Bains et al., 2015). Thus, PVN CRF cells must integrate upstream and downstream signals to positively and negatively gate their activity to allow the host to adaptively respond to stress (Kim et al., 2019). Relapse rates in those with AUD are high (~20–30% (Tuithof et al., 2013; Yamashita and Yoshioka, 2019)) and are greatly influenced by stress (Blaine and Sinha, 2017; Wemm et al., 2019). Despite this knowledge, no currently approved medications for AUD explicitly target the HPA axis (Haass-Koffler et al., 2018) or noradrenergic circuitry.

Chronic intermittent ethanol (CIE) exposure in rodents imposes behavioral changes that include loss of control over ethanol (EtOH) intake, anxiety-like behavior, and disruption of stress-coping behaviors (Kimbrough et al., 2017; Morales et al., 2015). For example, stress-induced increase in grooming, which helps calm an animal after exposure to a stressor, is lost following CIE (Marty et al., 2020b). However, even gold-standard preclinical models of AUD (such as CIE vapor exposure followed by protracted withdrawal) often result in a heterogeneity of drinking preferences within each experimental group (Logrip and Zorrilla, 2012; Morales et al., 2015; Okhuarobo et al., 2020). While exciting discoveries have started to uncover the neuronal underpinnings that contribute to compulsive escalation of alcohol intake leading to AUD (Domi et al., 2021), little is known about the contributions of repeated intoxication/withdrawal cycles to cellular dysfunction within the PVN during protracted withdrawal. This may have important implications for treating AUD, as prazosin (Praz) was found to be most efficacious in those with higher numbers of heavy drinking days (Wilcox et al., 2018).

CRF cells within the PVN are essential for both the function of the HPA axis and the gating of complex behaviors in response to environmental cues. For example, optogenetic inhibition of these cells results in increased rearing (an exploratory behavior) and decreased grooming (a stress-coping behavior) (Füzesi et al., 2016). Additionally, high frequency stimulation-evoked short-term glutamatergic plasticity (HFS-STP) within the PVN (Kuzmiski et al., 2010) has been shown to correspond to the animal's freezing response to a threatening stimulus (Daviu et al., 2020). We have previously demonstrated that CIE-induced loss of stress-induced HFS-STP within the PVN was due to increased N-methyl D-aspartate receptor (NMDA) subunit 2B (GluN2B) function, decreased CRF receptor 1 function, and altered intracellular phosphatase activity (Marty et al., 2020b). We have also shown that CIE-induced loss of stress-induced STP could be recovered by application of Praz in PNC recordings from male, but not female rats (Munier et al., 2022). Thus, furthering the understanding of the complex cellular mechanisms of PVN PNCs has potential to positively impact development of future pharmacotherapies for those afflicted with AUD.

Astrocytes have critical roles in K^+ buffering (Hübel and Ullah, 2016; Li et al., 2021), regulating synaptic strength (Hahn et al., 2015), recycling glutamate/glutamine (Andersen et al., 2021), amongst others (Khakh and Deneen, 2019), all of which influence the excitability of pre-and postsynaptic neurons. Astrocytes, together with the presynaptic neuronal terminal and the postsynaptic neuron comprise the "tripartite synapse", by which these components can communicate to alter signal transmission (reviewed in (Lalo et al., 2021a)). NE release in response to stressful stimuli gates a complex ATP-dependent neuronal-astrocytic crosstalk within the PVN to rapidly amplify glutamate transmission (Chen et al., 2019) specifically in males, which may be disrupted by CIE (Munier et al., 2022). However, the mechanisms by which astrocytic-neuronal crosstalk is impaired by CIE are currently not well understood.

Ca^{2+} imaging as a technique has gained significant traction over the past decade due to its ability to obtain large, rich data sets on many cell types (Hsiao et al., 2021; Yang and Yuste, 2017), due to Ca^{2+} flux's relation to intracellular second messenger signaling pathways and action potentials (Berridge, 1998; Schrank et al., 2020). *Ex-vivo*, high fidelity, single photon Ca^{2+} imaging has the added advantage of enabling rapid application of various electrical stimuli and pharmacological manipulations in a tightly controlled setting. We performed *ex-vivo,* single photon Ca^{2+} imaging in PVN slices subjected to a pharmacological stress protocol.

We were able to determine unique CIE-induced alterations in astrocytic and neuronal Ca^{2+} spike event frequency and kinetics throughout the different phases of our pharmacological stress protocol. We also used selective antagonists of α1AR, α2AR, and Glun2B-containing NMDAR, to determine the CIE-induced alterations and HFS-sensitivity of Ca^{2+} event frequency, and Ca^{2+} spike kinetics in PVN slices from control and CIE rats. Finally, we determined the similarities and differences between the relations of measured Ca^{2+} signaling profiles with CIE-associated behaviors.

2. Methods

2.1. Animals

All experiments were performed in accordance with the guidance of the National Institutes of Health on animal care and use and the University of California, Los Angeles Institutional Animal Care and Use Committee. Male Long-Evans rats (weighing 200–225 g) were pair-housed under 12-hr 6AM/6PM light/dark cycle with *ad libitum* access to food, water and environmental enrichment.

EtOH (Decon Laboratories, King of Prussia, PA) was administered via custom-built vapor chambers (La Jolla Alcohol Research, Inc.) for 12 h on/off cycles (on at 10PM), referred to as CIE (see Supplemental Methods (Munier et al., 2022)). Animals in their home cages passively consumed EtOH in gradually increasing doses throughout the 40-day experiment. Body weight was measured weekly to monitor potential adverse effects of EtOH exposure. Tail vein blood (30–50 μl) was collected into heparinized tubes (Microvette CB300, Starstedt, Germany) immediately following 12-hr vapor exposure during the last experimental week. Blood samples were centrifuged at 2000 g for 10 min at room temperature and the EtOH content of each sample measured in duplicate along with EtOH standards using the alcohol oxidase reaction procedure (GM7 Micro-Stat, Analox, Huntington Beach, CA). A cutoff of >150 mg/dl of EtOH in plasma was used to confirm that an intoxicating level of EtOH was reached in each rat (Getachew et al., 2008). Animals were subsequently withdrawn for a period of 30 days prior to behavioral assessment, which was employed to disentangle the persistent adaptations to the HPA axis seen previously (Richardson et al., 2008; Vendruscolo et al., 2012), from the effects of acute withdrawal. Room air-exposed, weight- and age-matched rats were used as controls.

2.2. Behavioral battery

Animals were given a behavioral battery to assess various stereotyped behaviors that have been associated with other preclinical models of AUD. Briefly, animals were allowed to acclimate to the room in their home cages for 30 min following room transfer and sessions started at 10AM. First, animals were videotaped in a clean, bare Plexiglass cage for 15 min. Grooming, stereotyped rostro caudal grooming transitions, and rearing were assessed by a blinded scorer (see Supplemental Methods (Kalueff et al., 2007)). Three days later, animals were given a 10-min open field test, digitally scored by EthoVision (Noldus, Leesburg, VA) software. The subsequent day, animals were exposed to 1 uncued foot-shock (1 mA, 1s) during an 8-min session with 2% Simple Green as an olfactory cue, blue polka dots as a visual cue, and metal bar flooring as a tactile cue. Animals were then reintroduced to the same context the next day to evaluate context-dependent fear during a 15-min session. Sessions were scored using Video Freeze (Med Associates Fairfax, VT) software. Finally, animals were given an intermittent access 2-bottle choice between potable water and 10% w/w EtOH, (see Supplemental Methods (Marty et al., 2020a; Meyer et al., 2013; Simms et al., 2008)).

2.3. Ca^{2+} imaging

CIE-exposed rats and their air-exposed controls were deeply anesthetized with isoflurane (Patterson Veterinary, MA, USA), decapitated and the brain removed and submerged in ice cold bubbling slicing artificial cerebrospinal fluid (ACSF) containing (in mM): 62 NaCl, 3.5 KCl, 1.25 NaH_2PO_4, 62 choline chloride, 0.5 $CaCl_2$, 3.5 $MgCl_2$, 26 $NaHCO_3$, 5 N-acetyl L-cysteine, and 5 glucose, pH adjusted to 7.3 with KOH. Acutely microdissected PVN slices (300 μm thick) were obtained (VT1200s, Leica, Buffalo Grove, IL) and transferred to room temperature normal ACSF containing (in mM): 125 NaCl, 2.5 KCl, 1.25 NaH_2PO_4, 2 $CaCl_2$, 2 $MgCl_2$, 26 $NaHCO_3$, 10 glucose, pH adjusted to 7.3 with KOH, and allowed equilibrate for >1 h prior to experimentation. Slices were then incubated in a 5-mL chamber containing ACSF, a cell-permeable Ca^{2+}-indicating dye, Calbryte 520AM (AAT Biosciences, Pleasanton, CA), DMSO (0.3% w/v), and pluronic acid (0.02% w/v) for 45–60 min and allowed to wash in another normal ACSF solution for >5 min prior to imaging. Calbryte 520AM is an esterified dye that, following cleavage after passive transport into the cytosol, exhibits greatly enhanced cellular retention without the need for additional pharmaceutical intervention (Liao et al., 2021).

Imaging was performed on a Scientifica SliceScope, with imaging components built on an Olympus BX51 upright fluorescence microscope equipped with an sCMOS camera (Hamamatsu Orca Flash 4.0v3). Slices were housed on poly-D lysine cover slips attached to a modified RC-26G chamber (Warner Instruments, Holliston, MA). Anatomical regions in brain sections for Ca^{2+} imaging were first identified by brightfield imaging with 780 nm LED (Scientifica, Clarksburg, NJ) illumination. Ca^{2+} imaging was performed using a 40x, 0.80NA water immersion objective (Olympus, TN, US), continuous 470 nm LED illumination (ThorLabs, Newton, NJ), and a filter cube suitable for Calbryte 520AM imaging: Excitation: Brightline 466/40, Dichroic: Semrock FF495-Di03, Emission: Brightline 525/50. Images were acquired continually with 20ms exposure time.

RC-26G was modified to house two platinum wires on opposing sides by which electric field stimulation could be applied using S88 stimulator and PSIU6 stimulus-isolation unit (Grass Instruments, West Warwick, RI). Electric field stimulation was applied at 110 mV (twin pulse every 5s. HFS was applied (100 Hz for 1 s, repeated four times with a 5 s interval) as previously described, except with field stimulation as opposed to a bipolar concentric stimulating electrode (see Supplemental Methods (Munier et al., 2022)). At the end of each experiment, slices were washed with high [K^+] ACSF, (containing in mM: 86 NaCl. 55.4 KCl, 1 $MgCl_2$, 0.33 NaH_2PO_4, 10 D-Glucose, 10 HEPES, 2 $CaCl_2$) to putatively discriminate between neuronal and astrocytic cell populations (Ravin et al., 2016). Temperature of ACSF during the recorded sessions was held at 28 °C to minimize bubble formation.

2.4. Drugs

Norepinephrine bitartrate (NE; Tocris Biosciences, Minneapolis, MN, #5169) was dissolved in distilled water at a stock concentration of 100 mM and diluted in ACSF to 10 μM. Selective α1AR antagonist, prazosin (Praz, Cayman Chemical, Ann Arbor, MI #15023) was dissolved in DMSO at a 10 mM stock concentration and diluted to a final volume of 10 μM in ACSF. Selective α2AR antagonist, atipamezole hydrochloride (Atip; Cayman Chemical, Ann Arbor, MI #34289) was dissolved in distilled water at a stock concentration of 50 mM, sonicated for 2 min, and diluted to a final concentration of 10 μM in ACSF. Selective GluN2b antagonist, Ro 25–6981 (Ro; Hellobio, Princeton, NJ #HB0554) was sonicated and dissolved in DMSO at a 5 mM stock concentration and diluted to a final volume of 5 μM in ACSF. Glucocorticoid receptor (GR) agonist, dexamethasone (DEX; Hellobio, Princeton, NJ, #HB2521) was dissolved in DMSO at a 5 mM stock concentration and diluted to a final volume of 5 μM in ACSF. Recordings were performed in the continuous presence of picrotoxin (50 μM; Hellobio, Princeton, NJ, #HB0506). All solutions were equilibrated at 28 ± 0.5 °C prior to slice application.

To mimic a pharmacologically mediated stress response, multiple PVN slices from the same animal were perfused with normal ACSF for 3 min, then NE, with or without selective antagonists (Praz, Atip, Ro) for a period of 8 min prior to imaging. Slices were then washed with normal ACSF again for 3 min prior to HFS of four trains at 100 Hz every 5 s to unmask STP of specific glutamatergic synapses onto PNCs. Subsequently, slices were perfused with DEX for 8 min and then washed with normal ACSF for 3 min to perform another round of HFS. Finally, slices were washed with high [K^+] ACSF, (containing in mM: 86 NaCl. 55.4 KCl, 1 $MgCl_2$, 0.33 NaH_2PO_4, 10 D-Glucose, 10 HEPES, 2 $CaCl_2$) to putatively discriminate between neuronal and astrocytic cell populations (Ravin et al., 2016).

2.5. Data extraction

Blinded scorers semi-manually curated regions of interest (ROIs) using Python-based Suite2P software (Pachitariu et al., 2017). ROI fluorescence was subtracted from the annual surround fluorescence, low-pass filtered, and transformed to dF/F (see Supplemental Methods (Asrican and Song, 2021)), where F_0 is calculated with a boxcar filter with a 200-frame lookback window. dF/F_0 values were clipped between 0 and 9000 to eliminate negative changes. Area under the curve and event frequency of each cell was calculated for each drug treatment. A threshold of 0.15 dF/F was used to determine significant events, which is lower than the dF/F of a single *ex-vivo* action potential (Tada et al., 2014), but significantly above signal to noise in our recorded traces. Kinetics analysis was performed on suprathreshold events following peak alignment and normalized to dF/F0 values 400ms before the peak (see Supplemental Methods).

2.6. Data analysis

All data are expressed as mean ± SEM. For behavioral and basal event frequency data, Student's t-test, Welch's *t*-test, or Mann-Whitney was used to evaluate differences between CIE and Air groups, when appropriate. Correlation was determined between behavioral variables using Pearson's correlation test. Multilevel models were used to determine the degree to which events (N = 31,540) and kinetics (N = 113,379) varied by phase of the pharmacological stress protocol (NE administration, HFS1, DEX administration, and HFS2 coded relative to baseline), differed by cell-type (0 = astrocyte, 1 = neuron), drug (Praz, Atip, Ro dummy-coded relative to NE), and treatment (0 = Air, 1 = CIE). Multilevel models act as an extension of regression that account for nesting within a cell or animal and allow for the number of observations to vary across nested clusters, enabling the statistical interpretation of our data together. Like a regression, each coefficient represents an individual contrast and therefore has 1 regression degree of freedom. Number of observations per model is reported in tables and figures. Post-hoc tests were tested using Tukey's honestly significant difference test. Correlation of behavioral variables with Ca^{2+} imaging measures were evaluated using Pearson's correlation test. Correlations were exploratory and were not corrected for family-wise error. GraphPad Prism 9 and Python Jupyter notebook was used for all data analyses. Alpha cutoff of 0.05 was used.

3. Results

3.1. CIE exposure alters hallmark behavioral traits and causes divergent relations between consummatory behaviors

Chronic exposure of rats to EtOH intoxication/withdrawal cycles results in behavioral changes, such as impaired flexibility, altered grooming, increased anxiety, and increased EtOH seeking/consumption (Fernandez et al., 2017; Kimbrough et al., 2017; Marty et al., 2020b; Morales et al., 2015). Still, it is appreciated that even "gold-standard"

preclinical models of AUD have considerable variability in the sought-after behavioral measures (i.e., EtOH intake, EtOH preference, etc.) within experimental groups (Logrip and Zorrilla, 2012; Morales et al., 2015; Okhuarobo et al., 2020) likely reflecting phenotypes underling susceptibility to these traits (Cloninger et al., 1988; Tawa et al., 2016). We employed a behavioral battery to broadly assess these measures in Air and CIE rats (Fig. 1a). CIE rats showed reduced grooming time (*p < 0.05; Fig. 1b) and Grooming:Rearing ratio (**p < 0.01; Fig. 1d), incorrect grooming transitions (****p < 0.0001; Fig. 1e) and increased rearing time (**p < 0.01; Fig. 1c) during video recording. CIE animals also displayed increased anxiety measures in terms of lower open field test velocity (*p < 0.05; Fig. 1f) and time spent in the center (**p < 0.01; Fig. 1g), without any differences in latency to the center (p > 0.05; Fig. 1h). CIE animals displayed increased weight adjusted EtOH consumption and preference (*p < 0.05; Fig. 1i and j), with considerable variability within both groups. When evaluating associative fear between Air and CIE groups, there was no detected statistical difference (p > 0.05; Fig. 1k). However, if we collapsed CIE and Air animals and re-segregated them into groups based on whether their preference for 10% EtOH w/v was >50% (alcohol preferring v. non-preferring, (*p < 0.05; Fig. 1l)), we found that non-preferring animals had more context-dependent fear (*p < 0.05; Fig. 1m).

Behavioral measures were then mapped for correlations amongst Air and CIE rats. Divergent patterns of behavioral traits relating to drinking behavior were uncovered. In Air controls, reactivity to a single foot-shock was negatively correlated with cumulative EtOH consumption across the 2-week period (Air * p < 0.05; Fig. 1n) and average EtOH preference was positively correlated with the latency to the center of the arena during the open field test (Air * p < 0.05; Fig. 1o). Together, these data suggest that CIE alters the behavioral profile of rats, which can be predictors of consummatory EtOH behavior.

3.2. *Pharmacological tools to assess the cellular mechanisms underlying CIE-induced HPA axis dysfunction in astrocytes and neurons*

NE and CORT are essential for the positive and negative gating of HPA axis activation, respectively. High-frequency stimulation (100 Hz) of afferents within the PVN produces a stress-dependent short-term potentiation of glutamatergic signaling (HFS-STP) (Kuzmiski et al., 2010) that has been linked to escape mechanisms in response to a looming shadow *in-vivo* (Daviu et al., 2020). Altered phosphatase activity in CIE drives maladaptive STP formation (Marty et al., 2020b), an effect which can be ameliorated (Munier et al., 2022) by antagonizing increased α1AR function (Varodayan et al., 2022) with Praz. Thus, we

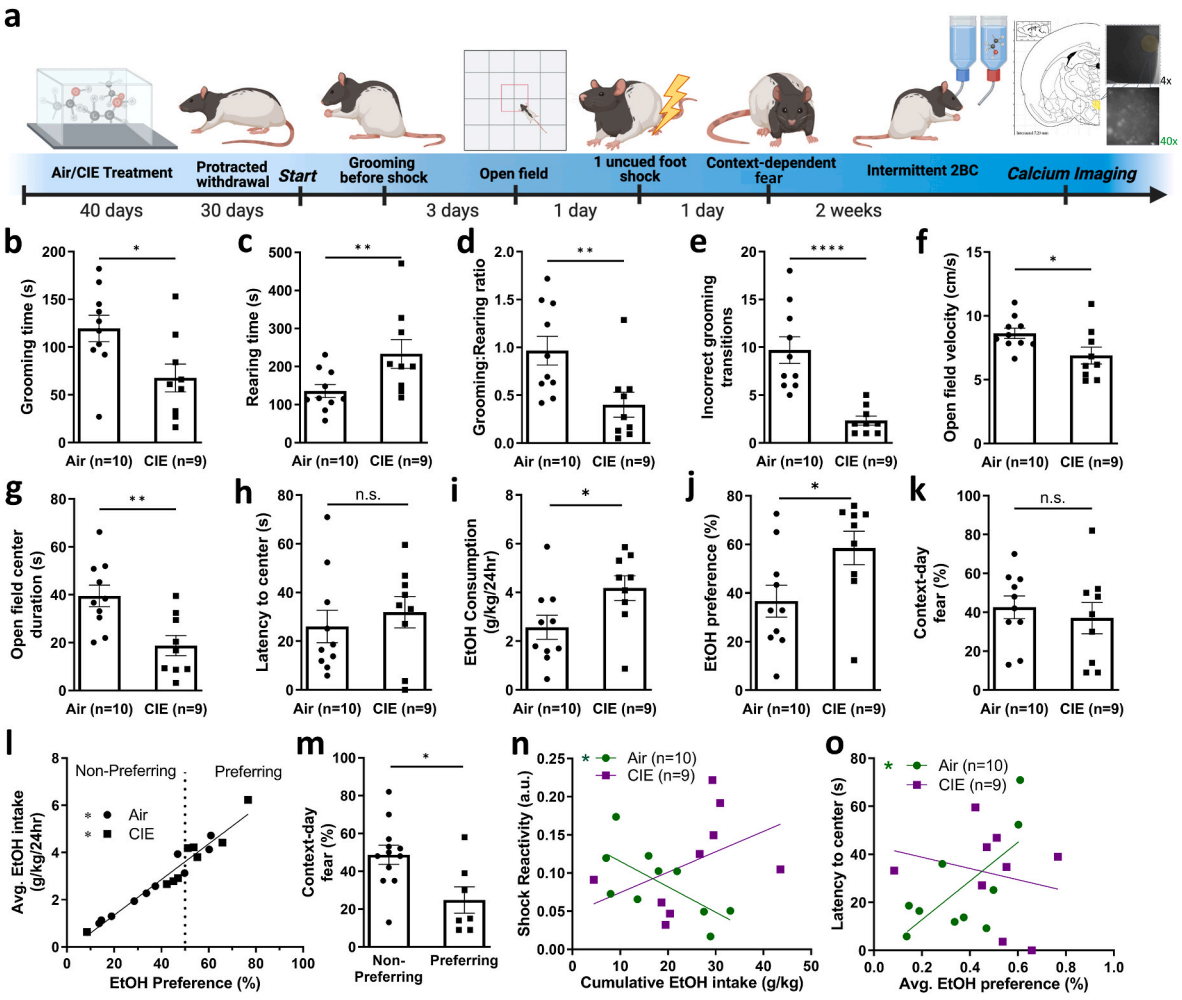

Fig. 1. CIE exposure alters hallmark behavioral traits and causes divergent relations between consummatory behaviors. a Pictorial timeline of treatment, behavior, and imaging protocol. **b** CIE decreases grooming time, **d** grooming:rearing ratio, **e** Incorrect grooming transitions, **f** open field velocity and **g** open field center duration. CIE increased **c** rearing, **h** EtOH consumption, and **j** preference over potable tap water. **k** No difference in context-dependent fear or **h** latency to the center in open field between Air and CIE rats. **l** Average EtOH intake and preference are correlated in both Air and CIE rats. **m** Rats with >50% EtOH preference show enhanced context-dependent fear. **n** Shock reactivity is negatively related to cumulative EtOH intake in Air rats. **o** Latency to the center of the open field is related to average EtOH preference in Air rats. Bar graphs represent mean±SEM. **b,f,g,h,i,m** Student's t-test; **c,d,e,j** Welch's *t*-test; **l, n, o** Linear regression. *p < 0.05, **p < 0.01, ****p < 0.0001.

employed single-photon Ca^{2+} imaging in *ex-vivo* PVN slices exposed to a pharmacological stress protocol (Fig. 2a), enabling the detection of drug-induced changes to stress-effector neurons and astrocytes. Each brain slice was treated with a brief application of 55.4 mM KCl-containing ACSF. Regions of interest were classified as putatively neuronal or astrocytic through succuss/failure to detect a supra-threshold Ca^{2+} event during the first 30s of 55.4 mM KCl-ACSF application. A simplified diagram displaying the known biochemical mechanisms underlying tripartite glutamate signaling in the PVN during various phases of HPA activation (Fig. 2b) is provided to clarify the assumed effects of our pharmacological manipulations.

3.3. CIE exposure alters the basal Ca^{2+} signaling and sensitivity to α1AR ligands in PVN neurons and astrocytes

AUD is characterized by inability to cope with relapse-inducing stressors. We have shown using electrophysiological methods that CIE alters the basal excitability and responsivity to NE in PNCs within the PVN (Munier et al., 2022). Astrocytes have complex roles in influencing neuronal signaling in a plethora of ways (Khakh and Deneen, 2019). Astrocytes also influence both neuronal PVN signaling (Chen et al., 2019) and acute (Erickson et al., 2021; Jin et al., 2021) and post-acute (Lindberg et al., 2019) effects of EtOH exposure. However, the contribution of astrocytes to CIE-induced alterations in neuronal signaling in response to NE (Munier et al., 2022) and during HFS-STP are not well-defined. Thus, we employed single-photon Ca^{2+} imaging to visualize responsivity to NE application with and without co-application of selective αAR antagonists of neuronal and astrocytic ROIs within *ex-vivo* slices.

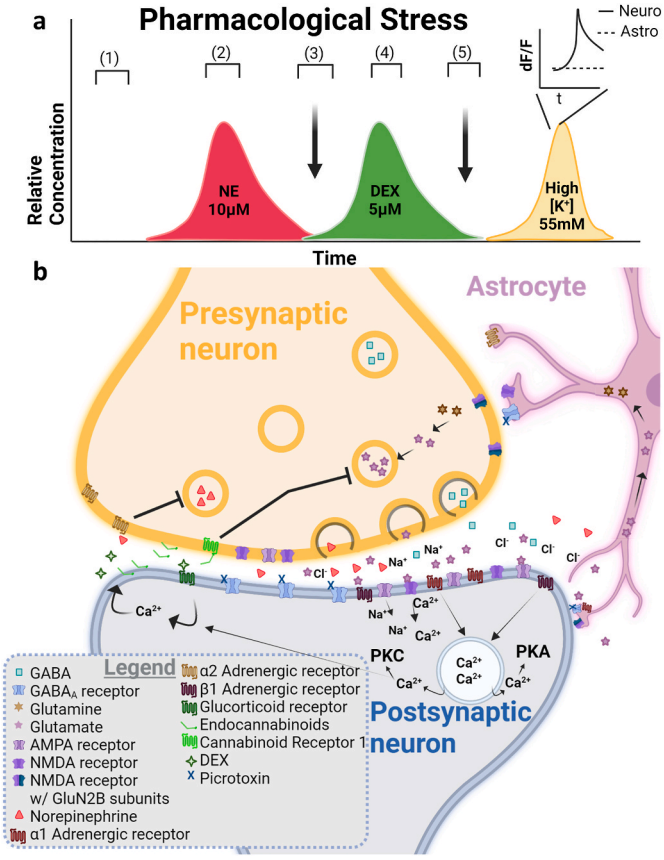

Fig. 2. Ex-vivo Ca^{2+} imaging during a pharmacological stress protocol enables investigation of tripartite mechanisms involved in stress responses. a Schematic of our sequential protocol composed of 5 phases: 1) Baseline, 2) NE administration, 3) HFS1, 4) DEX administration, 5) HFS2. Immediately prior to phases 3 and 5, an electric field stimulation was applied at 100 Hz for 5 s 4 times (HFS; black arrow). High $[K^+]$ ACSF was applied to distinguish between neuronal and astrocytic regions of interest. **b** A simplified schematic representation of the tripartite synapse to justify our pharmacological rationale.

CIE significantly decreased the frequency of suprathreshold Ca^{2+} events during the baseline phase of both neurons (****p < 0.0001, Fig. 3a1) and astrocytes (*p < 0.05, Fig. 3a2). In Air neurons, NE consistently reduced the event frequency, independent of which drug was co-applied with NE (*p < 0.05, Fig. 3b; ***p < 0.001, Fig. 3c; ***p < 0.001 Fig, 3d; ***p < 0.001 Fig. 3e). Further, CIE cells lacked NE-induced reductions in Ca^{2+} event frequency irrespective of drug treatment (p > 0.05, Fig. 3b, c, e), except those co-treated with Praz (***p < 0.001, Fig. 3d). Effects of drug treatment varied by cell-type, timing, and treatment. Specifically, the degree to which CIE affected associations between drug treatment and time varied between neurons and astrocytes for Atip during NE admin ($B = 2.57$, $SE = 1.15$, $*p = 0.026$), HFS1 ($B = 3.33$, $SE = 1.24$, $**p = 0.007$), and HFS2 ($B = 3.22$, $SE = 1.36$, $*p = 0.018$) and for Praz at HFS2 ($B = 2.37$, $SE = 1.00$, $*p = 0.017$). Associations were probed by examining differences for each drug type (results in Table S1). Co-application of Praz with NE was able to normalize these CIE-induced differences to NE-induced reduction in Ca^{2+} events in both cell types (***p < 0.001, Fig. 3d2). In cells where NE was co-applied with Atip, Ca^{2+} events were reduced in both Air astrocytes and neurons (***p < 0.001, Fig. 3c2). Co-application of Ro with NE blocked NE-induced reductions to Ca^{2+} events in Air astrocytes selectively (p > 0.05, Fig. 3e2). Together, these data suggest a selective dysfunction in α1AR signaling in CIE PVN cells during protracted withdrawal.

3.4. Drug and stimulation effects on tripartite Ca^{2+} signals are impacted by CIE exposure

We compared the effect of co-application of selective noradrenergic and glutamatergic receptor subtype antagonists on the frequency of Ca^{2+} events during our pharmacological stress protocol (Fig. 2a). Models assessed simple effects by examining the association between time and drug treatment for each combination of cell-type and experimental condition (CIE vs Air; results for each combination in Table S2). We determined that Air neurons treated with Praz enhanced NE's ability to reduce Ca^{2+} event frequency (***p < 0.001, Fig. 4a). Interestingly, Ro uncovered a relative increase compared to other treatment groups in Ca^{2+} events during HFS1, partially due to an aberrantly high basal event frequency (***p < 0.001, $$$ p < 0.001, #p < 0.05, Fig. 4a). This increase was absent during HFS2. Also, Praz uncovered an increase in the events of Air neurons during HFS2 compared to other treatment groups (***p < 0.001, $$$ p < 0.001, ###p < 0.001 Fig. 4a). A similar instance was seen for CIE neurons treated with Atip during HFS2 (***p < 0.001, ###p < 0.001 (Atip v. Praz & Ro), Fig. 4b). In Air astrocytes, Ro prevented relative (*p < 0.05, ###p < 0.001, $$$ p < 0.001, Fig. 4c) NE and (*p < 0.05, #p < 0.05, Fig. 4c) DEX-induced reductions to Ca^{2+} event frequency. Conversely, HFS2 unmasked a reduction in the events of these cells compared to NE-treated Air astrocytes (*p < 0.05, Fig. 4c). Praz enabled a selective increase in the Ca^{2+} events of CIE astrocytes during HFS2 (*p < 0.05, Fig. 4d). Together, these results demonstrate selective drug effects on specific cell types within the PVN throughout a pharmacological stress.

3.5. CIE alters HFS-induced changes to Ca^{2+} event kinetics in a drug and cell type-specific manner over pharmacological stress

Across phases, there was a significant interaction of Drug × CIE × Cell type × Time interaction, indicating that the degree to which time related to Ca^{2+}-spike peaks differed by treatment in a cell-specific manner for NE + Ro but not for other drug administrations ($B = -0.31$, $SE = 0.13$, $*p = 0.021$ for baseline versus drug administration, $B = -0.35$, $SE = 0.16$, $*p = 0.030$ for baseline versus DEX, $B = -0.38$, $SE = 0.15$, $*p = 0.013$ for baseline versus HFS1). The CIE × Time

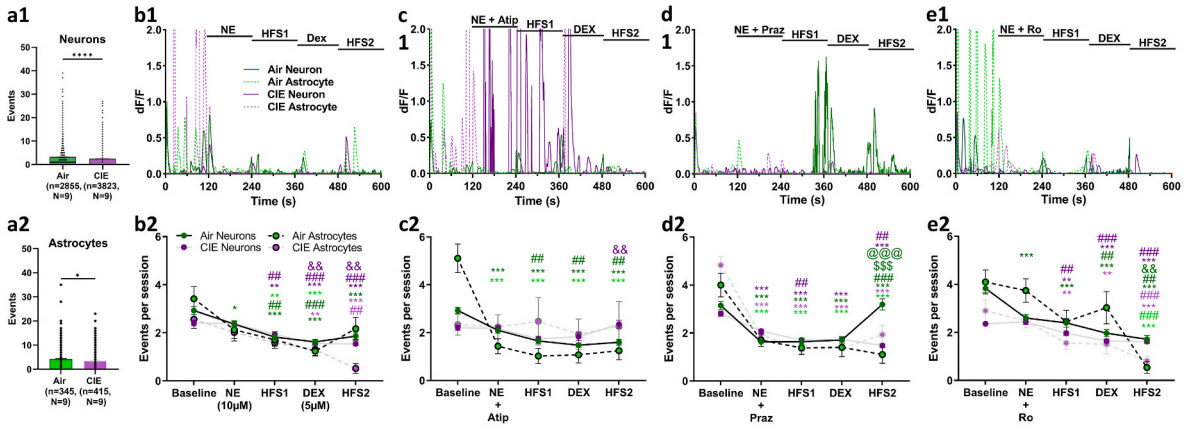

Fig. 3. CIE exposure alters the basal Ca^{2+} signaling and sensitivity to α1AR ligands in PVN neurons and astrocytes to alter tripartite communication. Basal events are reduced in both **a1** neurons and **a2** astrocytes by CIE treatment. **b1** Representative traces and **b2** quantification of events through the pharmacological stress protocol. **c1** Representative traces and **c2** quantification of events per phase during a pharmacological stress with co-application of Atip during NE administration. **d1** Representative traces and **d2** quantification of events per phase during a pharmacological stress with co-application of Praz during NE administration. **e1** Representative traces and **e2** quantification of events per phase during a pharmacological stress with co-application of Ro during NE administration. Line and bar graphs represent mean±SEM. **a** Mann-Whitney test. **b-e** Multi-level model. *p < 0.05, **p < 0.01, ***p < 0.001, *** difference from baseline. #p < 0.05, ##p < 0.01, ###p < 0.001 difference from NE administration. & p < 0.05, && p < 0.01, &&& p < 0.001 difference from HFS1.

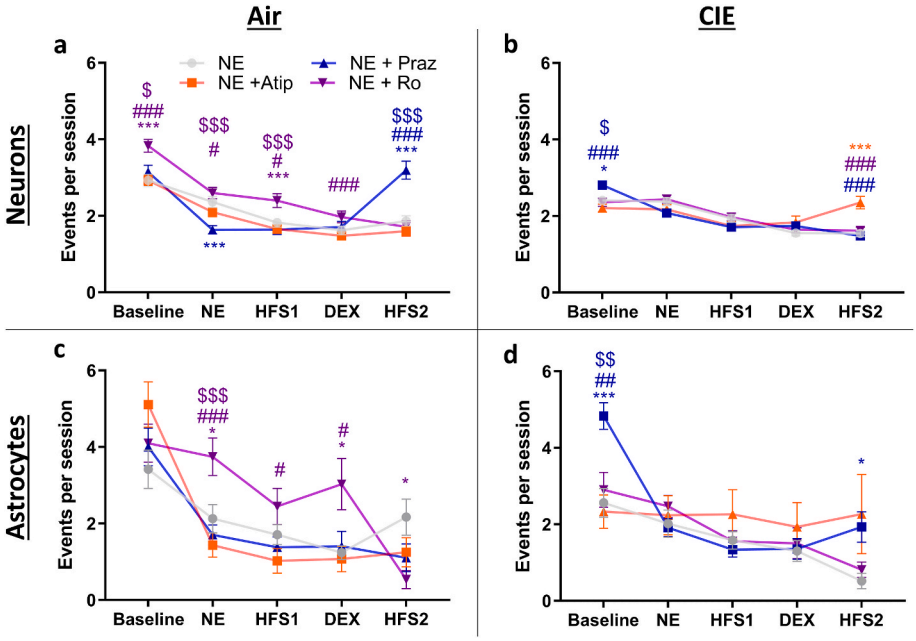

Fig. 4. αAR and NMDAR pharmacological manipulation imposes cell-type specific effects on Ca^{2+} event frequency. Quantification of Ca^{2+} events through our pharmacological stress protocol stratified by **a** air neurons, **b** CIE neurons, **c** Air astrocytes, and **d** CIE astrocytes. Line graphs represent mean±SEM. **a-d** Multi-level model. *p < 0.05, **p < 0.01, ***p < 0.001, difference from NE-treated, #p < 0.05, ##p < 0.01, ### difference from NE + Atip-treated, $ p < 0.05, $$ p < 0.01, $$$ p < 0.001, difference from NE + Praz-treated.

interactions were nonsignificant for astrocytes that were administered NE + Ro (*ps* > .09), such that these astrocytes in CIE showed higher peaks than in air irrespective of time ($B = 0.22$, $SE = 0.08$, $^{**}p = 0.003$; Fig. 5; Table S3). In contrast, the effects of CIE significantly differed by time for neurons and were related to greater peaks at baseline and more attenuated peaks at DEX and HFS1 (Fig. 6b1-c2; Table S3). The degree to which treatment impacted the time-dependent Ca^{2+} peak did not differ between astrocytes and neurons for other drug administrations, all *ps* > .17 (Supplemental Table S4).

Whereas differences in peak arose for Ro compared to other conditions, the degree to which time related to Ca^{2+}-spike anti-peaks differed by treatment in a cell-specific manner for NE + Praz but not for other drug administrations ($B = 1.12$, $SE = 0.46$, $^{*}p = 0.014$ at HFS1; $B = 1.16$, $SE = 0.44$, $^{**}p = 0.008$ at DEX; Table S5). Specifically, the effect of CIE on anti-peak differed between neurons and astrocyte at HFS1 ($B = 0.96$, $SE = 0.24$, $^{***}p < 0.001$) but not at DEX ($B = 0.24$, $SE = 0.29$, $p = 0.402$) for cells that were administered NE + Praz (Supplemental Table S5). CIE was related to a less negative anti-peak compared to air in astrocytes that were administered NE + Praz during HFS1 ($B = 0.74$, $SE = 0.36$, $^{*}p = 0.039$; Fig. 5d1-d2), but not in neurons ($B = -0.09$, $SE = 0.07$, $p = 0.206$; Fig. 6c1-c2). The opposite pattern was observed for cells that were administered NE, NE + Atip, and NE + Ro such that the effect of CIE on anti-peak differed between neurons and astrocyte at DEX ($B = -0.71$, $SE = 0.12$, $^{***}p < 0.001$) but not at HFS1 ($B = -0.01$, $SE = 0.10$, $p = 0.887$; Supplemental Table S6). During HFS1, CIE was related to a consistently more negative anti-peak for both neurons and astrocytes ($B = -0.05$, $SE = 0.02$, $^{*}p = 0.03$; Fig. 5c1-c2, 6b1-b2). During DEX, CIE was related to a more negative anti-peak for astrocytes ($B = -0.76$, $SE = 0.22$, $^{**}p = 0.001$; Fig. 5d1-5d2) but not neurons ($p = 0.142$; Fig. 6c1-c2).

To better assess these differences, we probed the significant interaction by examining the degree to which treatment affects drug-specific

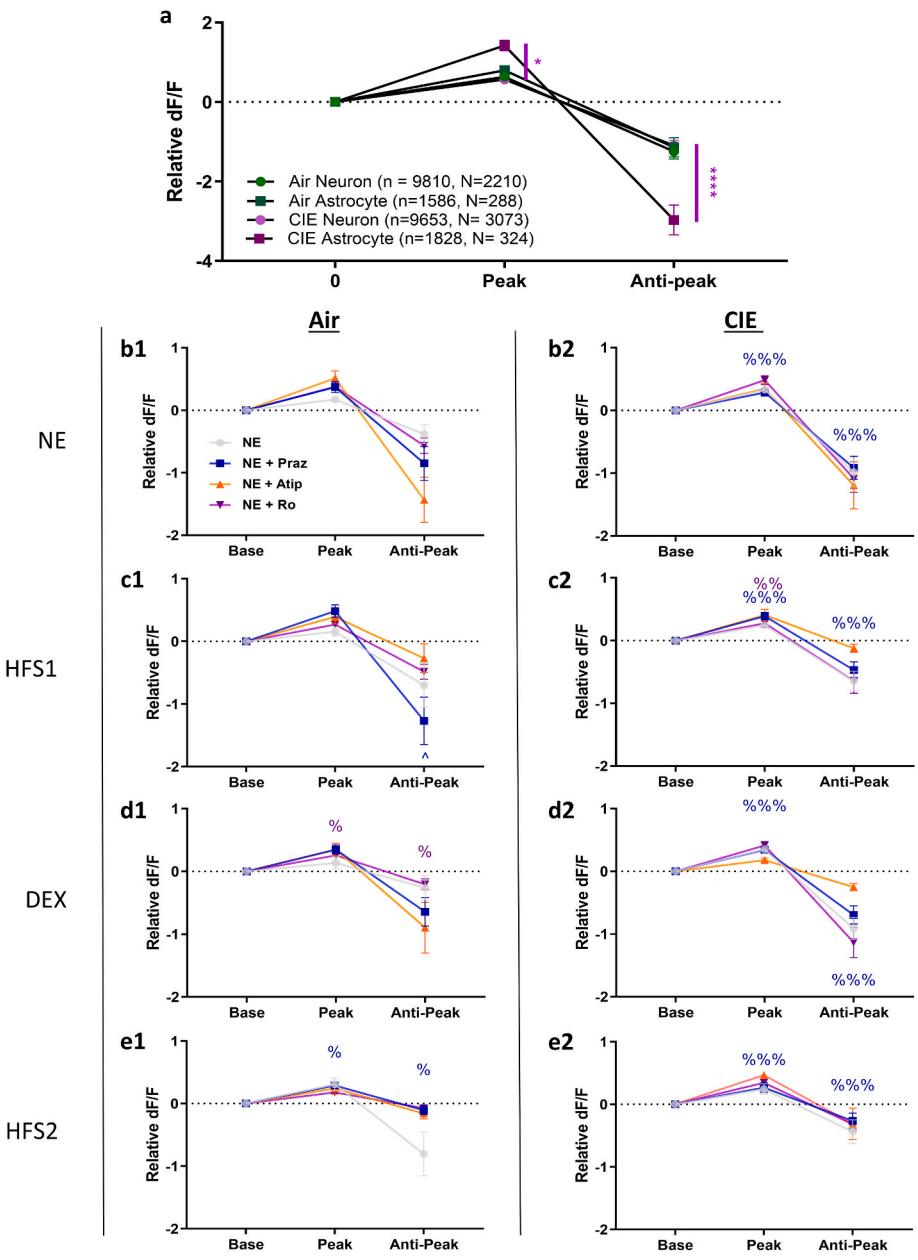

Fig. 5. PVN astrocyte Ca^{2+} kinetics are more robustly influenced by stimulation and neuroendocrine stress signaling in CIE rats. a CIE astrocytes have selectively elevated peaks and anti-peaks under basal conditions. **b1** Quantification of Air and **b2** CIE neuronal kinetics during NE administration. **c1** Assessment of the impact of HFS-STP on Air and **c2** CIE neurons. **d1** Quantification of Air and **d2** CIE neuronal kinetics during DEX administration. **e1** Assessment of the impact of HFS-STP on Air and **e2** CIE neurons following DEX administration. Line graphs represent mean±SEM. **a-e** Multi-level model. *p < 0.05, **p < 0.01, ***p < 0.001 differences amongst baselines. % p < 0.05, %% p < 0.01, %%% p < 0.001 difference from baseline, #p < 0.05, ##p < 0.01, ###p < 0.001 difference from DEX (from NE), ^ p < 0.05, ^^ p < 0.01, ^^^ p < 0.001 difference from HFS2 (from HFS1).

Ca^{2+} signaling across phases for astrocytes and then for neurons.

3.6. CIE alters HFS-induced changes to Ca^{2+} kinetics in astrocytes

HFS-induced changes to hypothalamic CRF neurons have been well-documented (Bains et al., 2015; Kuzmiski et al., 2010; Marty et al., 2011). However, the effects of this stimulation-induced plasticity on Ca^{2+} signaling are not well understood, particularly in astrocytes. This is despite the clear role astrocytes play in glutamate recycling (Andersen et al., 2021). We therefore investigated how our pharmacological stress protocol and HFS can may augment the kinetics of Ca^{2+} events in astrocytes within the PVN by normalizing all suprathreshold events to dF/F values @ t −400ms from the peak.

Astrocytes showed considerable treatment-specific changes in Ca^{2+} spike kinetics. Only CIE-treated astrocytes had larger peaks (*p < 0.05, Fig. 5a) and more pronounced after-peak reductions in Ca^{2+}, termed as an anti-peak for lack of a more specific term (****p < 0.0001, Fig. 5a). During NE treatment, the exaggerated peak of CIE astrocytic spikes was normalized (Fig. 5b2). Peaks and anti-peaks of Air astrocytes did not differ during any NE admin (Fig. 5b1), but NE + Praz uncovered a further decrease in peak and a less negative anti-peak of CIE astrocytes (%%% p < 0.001, Fig. 5b2). HFS1 had no significant effect on Air astrocytes post NE treatment (Fig. 5c1). CIE astrocytes showed a significantly reduced peak following NE + Ro and NE + Praz, (Praz: %%% p < 0.001; Ro: %% p < 0.01, Fig. 5c2). NE + Ro caused a reduction of peak and elevated anti-peak relative to baseline during the DEX phase (% p < 0.05, Fig. 5d1). HFS2 caused a more reduced peak and elevated anti-peak in only astrocytes treated with Praz (% p < 0.05, Fig. 5e1; %%% p < 0.001 Fig. 5e2), however this was significant to a larger extent in CIE-treated astrocytes. Together these data show stimulation's ability to modulate the kinetics of astrocytic Ca^{2+} spikes are dependent on the activation of noradrenergic and glucocorticoid receptors.

3.7. HFS-induced changes to Ca^{2+} kinetics in PVN neurons are influenced by both αAR and CIE

Metaplastic glutamate bursts (Kuzmiski et al., 2010) within the PVN are critical for escape decisions (Daviu et al., 2020). This response is

disrupted following CIE exposure (Marty et al., 2020b; Munier et al., 2022). However, it remains unclear how unmasking this metaplastic response affects acute Ca^{2+} signals in neurons and astrocytes. On one hand, it has been shown that postsynaptic Ca^{2+} chelation through BAPTA unmasked HFS-induced STP in PNCs (Kuzmiski et al., 2010). Seemingly paradoxically, both local glutamatergic signaling and action potentials increase intracellular [Ca^{2+}] of the postsynaptic cell (Tada et al., 2014). Thus, we sought to determine how our pharmacological stress protocol and HFS alters Ca^{2+} dynamics in neurons of Air and CIE rats.

Praz, Atip, and Ro all decreased the peak of Air neurons during NE administration (%%% $p < 0.001$, Fig. 6a1). NE and NE + Ro caused a less negative anti-peak in Air neurons (%%% $p < 0.001$, Fig. 6a1). CIE neurons treated with Praz or Atip showed a decreased peak and amplified anti-peak relative to baseline (%%% $p < 0.001$, Fig. 6a2). HFS1 decreased anti-peak of Atip neurons (%%% $p < 0.001$, Fig. 6b1), which was lost following CIE (Fig. 6b2). DEX decreased the peak in Praz, Atip and Ro co-treated neurons while decreasing the anti-peak in all groups to varying levels of significance (NE: % $p < 0.05$; Atip: %% $p < 0.01$; Praz: %%% $p < 0.001$; Ro: %%% $p < 0.001$; Fig. 6c1). CIE neuronal peak was only marginally diminished during DEX, but those cells that were previously treated with Praz showed a diminished peak and exaggerated anti-peak (%%% $p < 0.001$; Fig. 6c2). HFS2 uncovered a relative increase compared to HFS1 in the peak of NE and Praz-treated Air neurons (^^^ $p < 0.001$, Fig. 6b1). In CIE neurons during HFS2, there was instead a further reduction compared to HFS1 (^^^ $p < 0.001$, Fig. 6b2). Together, these results show that stimulation and drug administration rapidly alter the kinetics of neuronal Ca^{2+} signals and this is affected by CIE exposure.

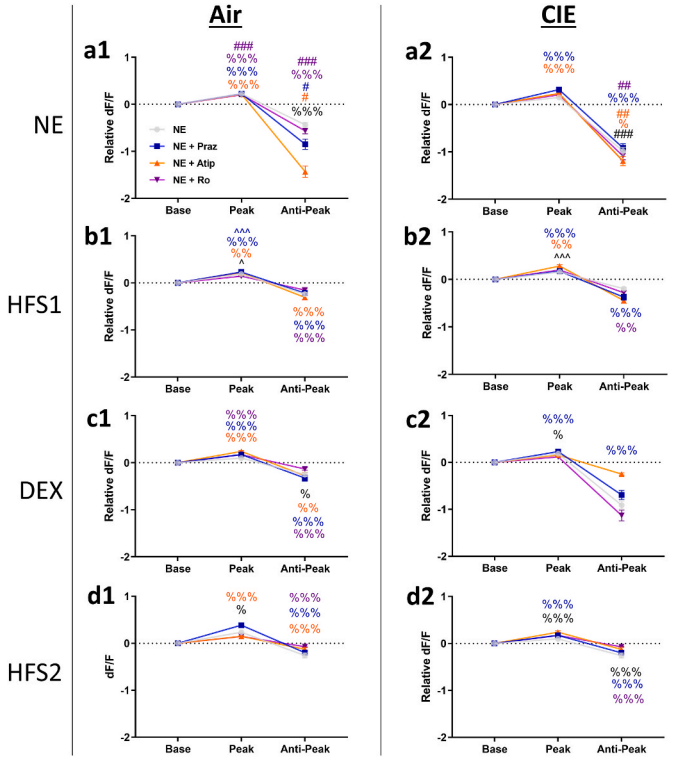

Fig. 6. CIE diminishes the dynamic flexibility of neuronal Ca^{2+} kinetics to neuroendocrine stress signals and stimulation. a1 Quantification of Air and **a2** CIE neuronal kinetics during NE administration. **b1** Assessment of the impact of HFS-STP on Air and **b2** CIE neurons. **c1** Quantification of Air and **c2** CIE neuronal kinetics during DEX administration. **d1** Assessment of the impact of HFS-STP on Air and **d2** CIE neurons following DEX administration. Line graphs represent mean±SEM. **a-d** Multi-level model. *$p < 0.05$, **$p < 0.01$, ***$p < 0.001$ differences amongst baselines. % $p < 0.05$, %% $p < 0.01$, %%% $p < 0.001$ difference from baseline, #$p < 0.05$, ##$p < 0.01$, ###$p < 0.001$ difference from DEX (from NE), ^ $p < 0.05$, ^^ $p < 0.01$, ^^^ $p < 0.001$ difference from HFS#2 (from HFS#1).

3.8. Behavioral test responses predict drug-induced changes to PVN neuronal activity during a pharmacological stress

It is unknown how interindividual differences in astrocytic and neuronal signaling in response to stress may influence the behavioral variance observed during assays. Given the varied cell-type specific responses to various pharmacological and stimulation-induced manipulations (Figs. 4–6), we performed an exploratory search of the parametric regressions of individual behaviors examined during our behavioral battery against the various physiological Ca^{2+} imaging measures. We identified some physiological features that corresponded to behavior, independent of CIE/Air treatment. For example, time spent rearing was significantly correlated with the extent to which neurons were inhibited during HFS#1 following NE treatment (**$p < 0.01$, Fig. 7a). Further, we found that the grooming:rearing ratio was correlated to the extent to which astrocytes were inhibited during NE (**$p < 0.01$, Fig. 7b). Additionally, the percent of neurons that were excited during NE + Ro was correlated to the percent of fear in the post-shock context test (**$p < 0.01$, Fig. 7c).

4. Discussion

Alcohol is known as an acute activator of the HPA axis (Rivier and Lee, 1996), whereas CIE exposure imposes a lasting toll on the resiliency of the HPA axis (Vendruscolo et al., 2012) and induces anxiety-like behaviors (Morales et al., 2015). Our recent work showed that CIE exposure impairs PVN PNC's plastic and metaplastic glutamatergic synaptic transmission and responses to norepinephrine (Marty et al., 2020b; Munier et al., 2022). Consistent with previous reports (Marty et al., 2020b), CIE animals exhibited decreased stress-coping behaviors, such as decreased time spent grooming. When CIE animals did groom, they showed more stereotyped rostro-caudal patterning (Kalueff et al., 2007), as exhibited through decreased incorrect grooming transitions. Additionally, CIE animals increased exploratory behavior (rearing) (Füzesi et al., 2016), as well as increased anxiety-associated behaviors (decreases in center duration and velocity) in the open-field assay (Prut and Belzung, 2003). CIE animals also responded to intermittent-access two-bottle choice with both higher mean consumption and preference for EtOH (Kimbrough et al., 2017; Morales et al., 2015). While CIE did not alter context fear *per se,* those that had a lower EtOH preference than 50% showed elevated levels of fear. The relationship of preference, anxiety and fear learning possibly supports previous evidence of CIE-induced alterations to hippocampus-amygdala circuitry (Liang et al., 2006; Lindemeyer et al., 2014; Price and McCool, 2022; Sizer et al., 2021), which mediates these affect-related behaviors (Maren and Fanselow, 1995; Zelikowsky et al., 2014). Finally, the relation of anxiety (latency to the center) and startle responses were significantly correlated to drinking behaviors only in Air rats, suggesting that CIE causes a shift in the factors that drive increased EtOH salience.

NE and glucocorticoids are essential for the positive and negative regulation of PVN CRF neuron activity, respectively (Cole and Sawchenko, 2002; Di et al., 2003). Here, we show that the ability of NE to decrease Ca^{2+} signaling in hypothalamic neurons is blunted in CIE rats. This supports previous findings that the ability of NE to suppress glutamatergic transmission is lost in CIE males (Munier et al., 2022). We also show that Praz blockade of α1AR normalizes neuronal Ca^{2+} responses to NE. This further supports our previous finding that Praz normalizes noradrenergic hyperactivity due to increased α1AR function in PVN CRF neurons of CIE males (Munier et al., 2022). By contrast, the synthetic GR agonist, DEX, was able to lower events from baseline in all groups except CIE males pretreated with Atip, suggesting that GR remains functional in CIE males. This also suggests that α2AR and GR reduce the frequency of Ca^{2+} events through redundant mechanisms to

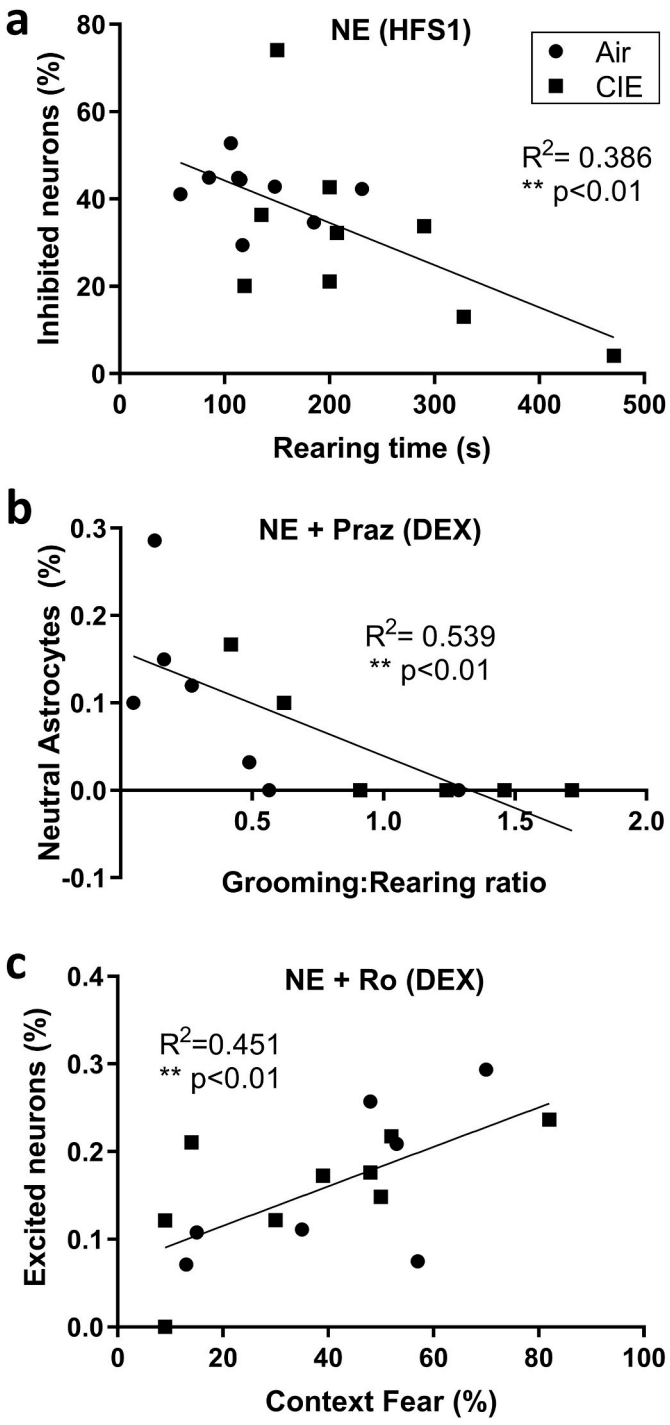

Fig. 7. Differences in stress-coping and affect-related behaviors are related to physiological Ca^{2+} responses in the PVN. a Exploratory rearing behavior during open field is negatively correlated to degree by which neurons were inhibited during HFS1 following NE administration. **b** Relative time spent between exploratory and stress-coping behaviors is positively correlated to the degree by astrocytes were unchanged during DEX following NE + PRAZ application. **c** Percentage of neurons excited during DEX following NE + Ro is positively related to context-dependent fear. **a-c** Linear regression. **p < 0.01.

suppress presynaptic glutamatergic transmission (Fig. 2b).

Previous studies have detailed that NE causes complex neuronal-astrocytic crosstalk to alter glutamatergic signaling in mouse PVN CRF neurons (Chen et al., 2019). Astrocytes play critical roles in the acute effects of EtOH intoxication (Jin et al., 2021), escalation of EtOH consumption (Erickson et al., 2021), and the post-acute effects of EtOH exposure, through astrocyte remodeling (Erickson et al., 2019). However, it is not known how CIE influences this neuronal-astrocytic crosstalk in the PVN, or how this may underlie the observed changes to neuronal signaling in response to pharmacological stress. Interestingly, like neurons, astrocytes from Air rats largely showed decreased Ca^{2+} event frequency in the presence of NE. The lone exception to this was in the co-presence of GluN2B antagonist, Ro. Previous studies showed that secreted factors from astrocytes can amplify the synaptic activity of GluN2B- containing NMDAR (Hahn et al., 2015). Our demonstration that selective blockade of GluN2B eliminates the NE-mediated reduction in astrocytic Ca^{2+} event frequency suggests that tonic neuronal GluN2B signaling is required to suppress astrocytic Ca^{2+} event frequency in response to neuroendocrine stress signals. This mechanism by which NE acts to suppress astrocytic Ca^{2+} signals may be upstream of GluN2B signaling, as astrocytes typically don't express this NMDAR subunit (Fig. 2b) (Lalo et al., 2021b; Savtchouk and Volterra, 2018). Like CIE neurons, only CIE astrocytes co-treated with Praz were able to decrease their event frequency in response to NE. Together, our data suggest that CIE causes a shift in reactivity of both neurons and astrocytes in response to excitatory and inhibitory neuroendocrine signals.

In multiple animal models, astrocytes have greater amplitude Ca^{2+} spike events than neurons (Asrican and Song, 2021; Chen et al., 2020). We replicate this here, giving us increased confidence in the ability to distinguish between astrocytic and neuronal Ca^{2+} signals. EtOH exposure can trigger glutamate release, reactive oxygen species formation (Salazar et al., 2008), amplify glucocorticoid induced Ca^{2+} accumulation (Mulholland et al., 2005), and induce gliosis of astrocytes of various brain regions, including the hypothalamus (Villavicencio-Tejo et al., 2021). Further, previous studies highlighted EtOH's ability to elicit Ca^{2+} signals in astrocytes and neurons *ex-vivo* (Kim et al., 2021). We found that CIE caused a greatly amplified astrocytic basal Ca^{2+} peak. There was also a greatly amplified anti-peak, which we took to indicate a refractory period between spikes. These amplified Ca^{2+} peaks/anti-peaks were normalized following NE administration, suggesting CIE-induced alterations in astrocytic AR function in protracted withdrawal. Indeed, many groups have highlighted a hyperadrenergic state in withdrawal (reviewed in Vazey et al., 2018). Both NE content (Varodayan et al., 2022) and basal release (Zhao et al., 2021) in CNS regions of rodents during protracted withdrawal from CIE are unchanged, further suggesting that the observed effects of NE application are due to altered astrocytic AR signaling. NE + Praz further suppressed the amplified peak and anti-peak of CIE astrocytes, highlighting a potential mechanism by which α1AR can be therapeutically targeted in CIE (Li et al., 2020).

While neuronal basal Ca^{2+} kinetics did not differ between Air or CIE groups, they displayed differences between drug treatments amongst the phases of the pharmacological stress protocol. NE administration was sufficient to reduce anti-peak only in Air neurons. NE + Ro reduced both peak and anti-peak only in Air neurons. Praz and Atip greatly reduced the peak and anti-peak of all neurons during NE administration. Generally, peaks and anti-peaks diminished in value across the pharmacological stress. However, CIE neurons failed to reduce anti-peak during DEX, suggesting potential differences in endocannabinoid synthesis (the byproduct of GR activation) of male rats as previously identified (Robinson et al., 2016).

We employed an exploratory search of potential convergent relationships between behavioral traits and relative proportions of excited and/or inhibited cells in Air and CIE-treated animals (see Supplemental Table 7). First, we found a relationship between time spent rearing and the percent neurons that were inhibited in response to HFS1 following NE administration. Previous studies have demonstrated the role of the PVN in rearing to explore environmental surroundings (Füzesi et al., 2016). Here, we further support these data and the notion that failure to properly engage metaplastic neuronal PVN signaling results in increased exploration of a neutral environment. However, the coordinated switch between grooming and rearing behavior *in vivo* may be mediated

through α1AR-dependent astrocytic-neuronal crosstalk. As such, there was a strong link between grooming:rearing and the fraction of neutral astrocytes following α1AR blockade during DEX administration. Separately, contextual fear has not been extensively linked to PVN behaviors. Still, we found a strong relationship between the percent of excited neurons following NE + Ro treatment during DEX administration and context fear. Further studies may examine the utility of GluN2B-specific mediated therapies for the treatment of contextual fear in other rigorous preclinical models.

There are important limitations of our study that should be noted. First, while visualizing Ca^{2+} signaling can be a suitable assay for assessing changes to synaptic activity (Berridge, 1998), it can also be directly affected by many other intracellular signaling cascades (Berridge, 1998), such as on-demand synthesis of endocannabinoids (Manz et al., 2020). Future studies could simultaneously record local field potentials to help differentiate between action potential-dependent and independent Ca^{2+} signals (Wu et al., 2021) in both neurons and astrocytes. Further, CIE-induced alterations to noradrenergic signaling are influenced by sex as a biological variable (Bangasser et al., 2016; Bangasser and Valentino, 2012; Bangasser and Wiersielis, 2018; Munier et al., 2022; Valentino et al., 2013). Future studies should examine the similarities and differences between females given an *ex-vivo* pharmacological stressor. Other incremental features could be added to the described methods, such as addition of two-photon microscopy systems, especially those that can automatedly survey multiple depths of an *ex-vivo* slice (Asrican and Song, 2021). Another limitation of the described study is that we did not gather data to evaluate the how transcriptomic identities of individual cellular populations within the PVN (Short et al., 2021) are specifically altered by CIE. Future studies coupling this technique with subsequent histological processes like CLARITY (Du et al., 2018) may enable researchers to rapidly evaluate pharmacological and stimulation-based mechanisms of synaptic dysfunction in multiple brain regions from the same animal with rich, biochemical detail.

In summary, we provide firm evidence that the cooperative function between astrocytes and neurons is disrupted following CIE vapor exposure and protracted withdrawal. These changes result in inadequate flexibility to respond to rapid increases in synaptic NE concentrations following exposure to a stressful stimulus, or other environmental factors that may activate the HPA axis, such as acute alcohol consumption (Rivier and Lee, 1996). This is likely due to increased neuronal α1AR since this was reversed in both neurons and astrocytes following treatment with Praz. Further, GluN2B blockade facilitated a normalized astrocytic Ca^{2+} event kinetics from CIE rats. Thus, polypharmacological approaches using α1AR and GluN2B antagonists may yield synergies in ameliorating dysfunctional hypothalamic tripartite signaling following CIE. Together, these findings provide key mechanistic insight towards pharmacotherapies that may ameliorate augmented anxiety-like behavioral responses to stressors in those afflicted with AUD.

Funding

The authors gratefully acknowledge the support of NIH/NIAAA [grant number R01AA026530] (MSF/IS), NIH/NIAAA [grant number AA024527] (IS), [grant number F31AA028183] (JJM), NIH/NIDA [grant number T32DA024635] (JJM), and NIH/NIDA [grant number K01DA042219] (PRO).

CRediT authorship contribution statement

J.J. Munier: conceptualized the project, completed data acquisition, performed data curation, performed formal statistical analyses. **S. Shen:** performed data curation, performed formal statistical analyses. **D. Rahal:** performed data curation, performed formal statistical analyses. **A. Hanna:** performed data curation. **V.N. Marty:** conceptualized the project. **P.R. O'Neill:** conceptualized the project. **M.S. Fanselow:** conceptualized the project. **I. Spigelman:** conceptualized the project.

Declaration of competing interest

The authors declare no competing financial interests.

Acknowledgements

We thank Kareem Kamal, Jasmine Pannu, Daniel Barrows and Megan Gomez for their assistance in data curation, ROI selection, and statistical analysis. We thank Sarah Gonzalez for training of proper recording of behavioral measures within the Fanselow Lab.

Appendix A. Supplementary data

Supplementary data to this article can be found online at https://doi.org/10.1016/j.ynstr.2023.100539.

References

Andersen, J.V., Markussen, K.H., Jakobsen, E., Schousboe, A., Waagepetersen, H.S., Rosenberg, P.A., Aldana, B.I., 2021. Glutamate metabolism and recycling at the excitatory synapse in health and neurodegeneration. Neuropharmacology 196, 108719. https://doi.org/10.1016/j.neuropharm.2021.108719.

Asrican, B., Song, J., 2021. Extracting meaningful circuit-based calcium dynamics in astrocytes and neurons from adult mouse brain slices using single-photon GCaMP imaging. STAR Protoc. 2, 100306 https://doi.org/10.1016/j.xpro.2021.100306.

Bains, J.S., Cusulin, J.I.W., Inoue, W., 2015. Stress-related synaptic plasticity in the hypothalamus. Nat. Rev. Neurosci. 16, 377–388. https://doi.org/10.1038/nrn3881.

Bangasser, D.A., Valentino, R.J., 2012. Sex differences in molecular and cellular substrates of stress. Cell. Mol. Neurobiol. 32, 709–723. https://doi.org/10.1007/s10571-012-9824-4.

Bangasser, D.A., Wiersielis, K.R., 2018. Sex differences in stress responses: a critical role for corticotropin-releasing factor. Hormones (Basel) 17, 5–13. https://doi.org/10.1007/s42000-018-0002-z.

Bangasser, D.A., Wiersielis, K.R., Khantsis, S., 2016. Sex differences in the locus coeruleus-norepinephrine system and its regulation by stress. Brain Res. 1641, 177–188. https://doi.org/10.1016/j.brainres.2015.11.021.

Berridge, M.J., 1998. Neuronal calcium signaling. Neuron 21, 13–26. https://doi.org/10.1016/s0896-6273(00)80510-3.

Blaine, S.K., Sinha, R., 2017. Alcohol, stress, and glucocorticoids: from risk to dependence and relapse in alcohol use disorders. Neuropharmacology 122, 136–147. https://doi.org/10.1016/j.neuropharm.2017.01.037.

Blanco, C., Iza, M., Rodríguez-Fernández, J.M., Baca-García, E., Wang, S., Olfson, M., 2015. Probability and predictors of treatment-seeking for substance use disorders in the U.S. Drug Alcohol Depend. 149, 136–144. https://doi.org/10.1016/j.drugalcdep.2015.01.031.

Chen, C., Jiang, Z., Fu, X., Yu, D., Huang, H., Tasker, J.G., 2019. Astrocytes amplify neuronal dendritic volume transmission stimulated by norepinephrine. Cell Rep. 29, 4349–4361.e4. https://doi.org/10.1016/j.celrep.2019.11.092.

Chen, J., Poskanzer, K.E., Freeman, M.R., Monk, K.R., 2020. Live-imaging of astrocyte morphogenesis and function in zebrafish neural circuits. Nat. Neurosci. 23, 1297–1306. https://doi.org/10.1038/s41593-020-0703-x.

Cloninger, C.R., Sigvardsson, S., Knorring, A.-L., Bohman, M., 1988. The Swedish studies of the adopted children of alcoholics: a reply to littrell. J. Stud. Alcohol 49, 500–509. https://doi.org/10.15288/jsa.1988.49.500.

Cole, R.L., Sawchenko, P.E., 2002. Neurotransmitter regulation of cellular activation and neuropeptide gene expression in the paraventricular nucleus of the hypothalamus. J. Neurosci. 22, 959–969. https://doi.org/10.1523/JNEUROSCI.22-03-00959.2002.

Daviu, N., Füzesi, T., Rosenegger, D.G., Rasiah, N.P., Sterley, T.-L., Peringod, G., Bains, J. S., 2020. Paraventricular nucleus CRH neurons encode stress controllability and regulate defensive behavior selection. Nat. Neurosci. 23, 398–410. https://doi.org/10.1038/s41593-020-0591-0.

Di, S., Malcher-Lopes, R., Halmos, K.Cs, Tasker, J.G., 2003. Nongenomic glucocorticoid inhibition via endocannabinoid release in the hypothalamus: a fast feedback mechanism. J. Neurosci. 23, 4850. https://doi.org/10.1523/JNEUROSCI.23-12-04850.2003. LP – 4857.

Domi, E., Xu, L., Toivainen, S., Nordeman, A., Gobbo, F., Venniro, M., Shaham, Y., Messing, R.O., Visser, E., van den Oever, M.C., Holm, L., Barbier, E., Augier, E., Heilig, M., 2021. A neural substrate of compulsive alcohol use. Sci. Adv. 7 https://doi.org/10.1126/sciadv.abg9045.

Du, H., Hou, P., Zhang, W., Li, Q., 2018. Advances in CLARITY-based tissue clearing and imaging. Exp. Ther. Med. 16, 1567–1576. https://doi.org/10.3892/etm.2018.6374.

Erickson, E.K., Blednov, Y.A., Harris, R.A., Mayfield, R.D., 2019. Glial gene networks associated with alcohol dependence. Sci. Rep. 9, 10949 https://doi.org/10.1038/s41598-019-47454-4.

Erickson, E.K., DaCosta, A.J., Mason, S.C., Blednov, Y.A., Mayfield, R.D., Harris, R.A., 2021. Cortical astrocytes regulate ethanol consumption and intoxication in mice. Neuropsychopharmacology 46, 500–508. https://doi.org/10.1038/s41386-020-0721-0.

Fernandez, G.M., Lew, B.J., Vedder, L.C., Savage, L.M., 2017. Chronic intermittent ethanol exposure leads to alterations in brain-derived neurotrophic factor within the frontal cortex and impaired behavioral flexibility in both adolescent and adult rats. Neuroscience 348, 324–334. https://doi.org/10.1016/j.neuroscience.2017.02.045.

Füzesi, T., Daviu, N., Wamsteeker Cusulin, J.I., Bonin, R.P., Bains, J.S., 2016. Hypothalamic CRH neurons orchestrate complex behaviours after stress. Nat. Commun. 7, 11937 https://doi.org/10.1038/ncomms11937.

Getachew, B., Hauser, S.R., Taylor, R.E., Tizabi, Y., 2008. Desipramine blocks alcohol-induced anxiety- and depressive-like behaviors in two rat strains. Pharmacol. Biochem. Behav. 91, 97–103. https://doi.org/10.1016/j.pbb.2008.06.016.

Haass-Koffler, C.L., Swift, R.M., Leggio, L., 2018. Noradrenergic targets for the treatment of alcohol use disorder. Psychopharmacology (Berl) 235, 1625–1634. https://doi.org/10.1007/s00213-018-4843-6.

Hahn, J., Wang, X., Margeta, M., 2015. Astrocytes increase the activity of synaptic GluN2B NMDA receptors. Front. Cell. Neurosci. 9, 117. https://doi.org/10.3389/fncel.2015.00117.

Heilig, M., Sommer, W.H., Spanagel, R., 2016. The need for treatment responsive translational biomarkers in alcoholism Research. Curr. Top. Behav. Neurosci. 28, 151–171. https://doi.org/10.1007/7854_2015_5006.

Hsiao, Y.-T., Wang, A.Y.-C., Lee, T.-Y., Chang, C.-Y., 2021. Using baseplating and a miniscope preanchored with an objective lens for calcium transient Research in mice. J. Vis. Exp. https://doi.org/10.3791/62611.

Hübel, N., Ullah, G., 2016. Anions govern cell volume: a case study of relative astrocytic and neuronal swelling in spreading depolarization. PLoS One 11, e0147060.

Jin, S., Cao, Q., Yang, F., Zhu, H., Xu, S., Chen, Q., Wang, Z., Lin, Y., Cinar, R., Pawlosky, R.J., Zhang, Y., Xiong, W., Gao, B., Koob, G.F., Lovinger, D.M., Zhang, L., 2021. Brain ethanol metabolism by astrocytic ALDH2 drives the behavioural effects of ethanol intoxication. Nat. Metab. 3, 337–351. https://doi.org/10.1038/s42255-021-00357-z.

Kalueff, A.V., Aldridge, J.W., LaPorte, J.L., Murphy, D.L., Tuohimaa, P., 2007. Analyzing grooming microstructure in neurobehavioral experiments. Nat. Protoc. 2, 2538–2544. https://doi.org/10.1038/nprot.2007.367.

Khakh, B.S., Deneen, B., 2019. The emerging nature of astrocyte diversity. Annu. Rev. Neurosci. 42, 187–207. https://doi.org/10.1146/annurev-neuro-070918-050443.

Kim, H.-B., Morris, J., Miyashiro, K., Lehto, T., Langel, Ü., Eberwine, J., Sul, J.-Y., 2021. Astrocytes promote ethanol-induced enhancement of intracellular Ca2+ signals through intercellular communication with neurons. iScience 24, 102436. https://doi.org/10.1016/j.isci.2021.102436.

Kim, J., Lee, S., Fang, Y.-Y., Shin, A., Park, S., Hashikawa, K., Bhat, S., Kim, D., Sohn, J.-W., Lin, D., Suh, G.S.B., 2019. Rapid, biphasic CRF neuronal responses encode positive and negative valence. Nat. Neurosci. 22, 576–585. https://doi.org/10.1038/s41593-019-0342-2.

Kimbrough, A., Kim, S., Cole, M., Brennan, M., George, O., 2017. Intermittent access to ethanol drinking facilitates the transition to excessive drinking after chronic intermittent ethanol vapor exposure. Alcohol Clin. Exp. Res. 41, 1502–1509. https://doi.org/10.1111/acer.13434.

Kuzmiski, J.B., Marty, V., Baimoukhametova, D. v, Bains, J.S., 2010. Stress-induced priming of glutamate synapses unmasks associative short-term plasticity. Nat. Neurosci. 13, 1257–1264. https://doi.org/10.1038/nn.2629.

Lalo, U., Koh, W., Lee, C.J., Pankratov, Y., 2021a. The tripartite glutamatergic synapse. Neuropharmacology 199, 108758. https://doi.org/10.1016/j.neuropharm.2021.108758.

Lalo, U., Koh, W., Lee, C.J., Pankratov, Y., 2021b. The tripartite glutamatergic synapse. Neuropharmacology 199, 108758. https://doi.org/10.1016/j.neuropharm.2021.108758.

Li, H., Lones, L., DiAntonio, A., 2021. Bidirectional regulation of glial potassium buffering - gliioprotection versus neuroprotection. Elife 10. https://doi.org/10.7554/eLife.62606.

Li, J., Wang, H., Li, M., Shen, Q., Li, X., Rong, X., Peng, Y., 2020. Efficacy of pharmacotherapeutics for patients comorbid with alcohol use disorders and depressive symptoms—a bayesian network meta-analysis. CNS Neurosci. Ther. 26, 1185–1197. https://doi.org/10.1111/cns.13437.

Liang, J., Zhang, N., Cagetti, E., Houser, C.R., Olsen, R.W., Spigelman, I., 2006. Chronic intermittent ethanol-induced switch of ethanol actions from extrasynaptic to synaptic hippocampal GABA $_A$ receptors. J. Neurosci. 26, 1749–1758. https://doi.org/10.1523/JNEUROSCI.4702-05.2006.

Liao, J., Patel, D., Zhao, Q., Peng, R., Guo, H., Diwu, Z., 2021. A novel Ca2+ indicator for long-term tracking of intracellular calcium flux. Biotechniques 70, 271–277. https://doi.org/10.2144/btn-2020-0161.

Lindberg, D., Ho, A.M.C., Peyton, L., Choi, D.-S., 2019. Chronic ethanol exposure disrupts lactate and glucose homeostasis and induces dysfunction of the astrocyte-neuron lactate shuttle in the brain. Alcohol Clin. Exp. Res. 43, 1838–1847. https://doi.org/10.1111/acer.14137.

Lindemeyer, A.K., Liang, J., Marty, V.N., Meyer, E.M., Suryanarayanan, A., Olsen, R.W., Spigelman, I., 2014. Ethanol-induced plasticity of GABAA receptors in the basolateral amygdala. Neurochem. Res. 39, 1162–1170. https://doi.org/10.1007/s11064-014-1297-z.

Logrip, M.L., Zorrilla, E.P., 2012. Stress history increases alcohol intake in relapse: relation to phosphodiesterase 10A. Addiction Biol. 17, 920–933. https://doi.org/10.1111/j.1369-1600.2012.00460.x.

Manz, K.M., Ghose, D., Turner, B.D., Taylor, A., Becker, J., Grueter, C.A., Grueter, B.A., 2020. Calcium-permeable AMPA receptors promote endocannabinoid signaling at parvalbumin interneuron synapses in the nucleus accumbens core. Cell Rep. 32, 107971 https://doi.org/10.1016/j.celrep.2020.107971.

Maren, S., Fanselow, M., 1995. Synaptic plasticity in the basolateral amygdala induced by hippocampal formation stimulation in vivo. J. Neurosci. 15, 7548–7564. https://doi.org/10.1523/JNEUROSCI.15-11-07548.1995.

Marty, V., Kuzmiski, J.B., Baimoukhametova, D. v, Bains, J.S., 2011. Short-term plasticity impacts information transfer at glutamate synapses onto parvocellular neuroendocrine cells in the paraventricular nucleus of the hypothalamus. J. Physiol. 589, 4259–4270. https://doi.org/10.1113/jphysiol.2011.208082.

Marty, V.N., Farokhnia, M., Munier, J.J., Mulpuri, Y., Leggio, L., Spigelman, I., 2020a. Long-acting glucagon-like peptide-1 receptor agonists suppress voluntary alcohol intake in male wistar rats. Front. Neurosci. 14, 599646 https://doi.org/10.3389/fnins.2020.599646.

Marty, V.N., Mulpuri, Y., Munier, J.J., Spigelman, I., 2020b. Chronic alcohol disrupts hypothalamic responses to stress by modifying CRF and NMDA receptor function. Neuropharmacology 167, 107991. https://doi.org/10.1016/j.neuropharm.2020.107991.

Meyer, E.M., Long, V., Fanselow, M.S., Spigelman, I., 2013. Stress increases voluntary alcohol intake, but does not alter established drinking habits in a rat model of posttraumatic stress disorder. Alcohol Clin. Exp. Res. 37, 566–574. https://doi.org/10.1111/acer.12012.

Morales, M., McGinnis, M.M., McCool, B.A., 2015. Chronic ethanol exposure increases voluntary home cage intake in adult male, but not female, Long-Evans rats. Pharmacol. Biochem. Behav. 139, 67–76. https://doi.org/10.1016/j.pbb.2015.10.016.

Mulholland, P.J., Self, R.L., Harris, B.R., Little, H.J., Littleton, J.M., Prendergast, M.A., 2005. Corticosterone increases damage and cytosolic calcium accumulation associated with ethanol withdrawal in rat hippocampal slice cultures. Alcohol Clin. Exp. Res. 29, 871–881. https://doi.org/10.1097/01.ALC.0000163509.27577.DA.

Munier, J.J., Marty, V.N., Spigelman, I., 2022. Sex differences in α-adrenergic receptor function contribute to impaired hypothalamic metaplasticity following chronic intermittent ethanol exposure. Alcohol Clin. Exp. Res. https://doi.org/10.1111/acer.14900.

Okhuarobo, A., Bolton, J.L., Igbe, I., Zorrilla, E.P., Baram, T.Z., Contet, C., 2020. A novel mouse model for vulnerability to alcohol dependence induced by early-life adversity. Neurobiol. Stress 13, 100269. https://doi.org/10.1016/j.ynstr.2020.100269.

Pachitariu, M., Stringer, C., Dipoppa, M., Schröder, S., Rossi, L.F., Dalgleish, H., Carandini, M., Harris, K.D., 2017. Suite2p: beyond 10,000 neurons with standard two-photon microscopy. bioRxiv, 061507. https://doi.org/10.1101/061507.

Peltier, M.R., Verplaetse, T.L., Mineur, Y.S., Petrakis, I.L., Cosgrove, K.P., Picciotto, M.R., McKee, S.A., 2019. Sex differences in stress-related alcohol use. Neurobiol. Stress 10, 100149. https://doi.org/10.1016/j.ynstr.2019.100149.

Price, M.E., McCool, B.A., 2022. Chronic alcohol dysregulates glutamatergic function in the basolateral amygdala in a projection-and sex-specific manner. Front. Cell. Neurosci. 16 https://doi.org/10.3389/fncel.2022.857550.

Prut, L., Belzung, C., 2003. The open field as a paradigm to measure the effects of drugs on anxiety-like behaviors: a review. Eur. J. Pharmacol. 463, 3–33. https://doi.org/10.1016/s0014-2999(03)01272-x.

Ravin, R., Blank, P.S., Busse, B., Ravin, N., Vira, S., Bezrukov, L., Waters, H., Guerrero-Cazares, H., Quinones-Hinojosa, A., Lee, P.R., Fields, R.D., Bezrukov, S.M., Zimmerberg, J., 2016. Blast shockwaves propagate Ca2+ activity via purinergic astrocyte networks in human central nervous system cells. Sci. Rep. 6, 25713 https://doi.org/10.1038/srep25713.

Richardson, H.N., Lee, S.Y., O'Dell, L.E., Koob, G.F., Rivier, C.L., 2008. Alcohol self-administration acutely stimulates the hypothalamic-pituitary- adrenal axis, but alcohol dependence leads to a dampened neuroendocrine state. Eur. J. Neurosci. 28, 1641–1653. https://doi.org/10.1111/j.1460-9568.2008.06455.x.

Rivier, C., Lee, S., 1996. Acute alcohol administration stimulates the activity of hypothalamic neurons that express corticotropin-releasing factor and vasopressin. Brain Res. 726, 1–10. https://doi.org/10.1016/0006-8993(96)00301-0.

Robinson, S.L., Alexander, N.J., Bluett, R.J., Patel, S., McCool, B.A., 2016. Acute and chronic ethanol exposure differentially regulate CB1 receptor function at glutamatergic synapses in the rat basolateral amygdala. Neuropharmacology 108, 474–484. https://doi.org/10.1016/j.neuropharm.2015.12.005.

Sacks, J.J., Gonzales, K.R., Bouchery, E.E., Tomedi, L.E., Brewer, R.D., 2015. 2010 national and state costs of excessive alcohol consumption. Am. J. Prev. Med. 49, e73–e79. https://doi.org/10.1016/j.amepre.2015.05.031.

Salazar, M., Pariente, J.A., Salido, G.M., González, A., 2008. Ethanol induces glutamate secretion by Ca2+ mobilization and ROS generation in rat hippocampal astrocytes. Neurochem. Int. 52, 1061–1067. https://doi.org/10.1016/j.neuint.2007.11.001.

Savtchouk, I., Volterra, A., 2018. Gliotransmission: beyond black-and-white. J. Neurosci. 38 (14) https://doi.org/10.1523/JNEUROSCI.0017-17.2017. LP – 25.

Schrank, S., Barrington, N., Stutzmann, G.E., 2020. Calcium-handling defects and neurodegenerative disease. Cold Spring Harbor Perspect. Biol. 12 https://doi.org/10.1101/cshperspect.a035212.

Short, A.K., Thai, C.W., Chen, Y., Kamei, N., Pham, A.L., Birnie, M.T., Bolton, J.L., Mortazavi, A., Baram, T.Z., 2021. Single-cell transcriptional changes in hypothalamic corticotropin-releasing factor–expressing neurons after early-life adversity inform enduring alterations in vulnerabilities to stress. Biol. Psychiatry Glob. Open Sci. https://doi.org/10.1016/j.bpsgos.2021.12.006.

Simms, J.A., Steensland, P., Medina, B., Abernathy, K.E., Chandler, L.J., Wise, R., Bartlett, S.E., 2008. Intermittent access to 20% ethanol induces high ethanol consumption in long–evans and wistar rats. Alcohol Clin. Exp. Res. 32, 1816–1823. https://doi.org/10.1111/j.1530-0277.2008.00753.x.

Sizer, S.E., Parrish, B.C., McCool, B.A., 2021. Chronic ethanol exposure potentiates cholinergic neurotransmission in the basolateral amygdala. Neuroscience 455, 165–176. https://doi.org/10.1016/j.neuroscience.2020.12.014.

Smith, S.M., Vale, W.W., 2006. The role of the hypothalamic-pituitary-adrenal axis in neuroendocrine responses to stress. Dialogues Clin. Neurosci. 8, 383–395.
Tada, M., Takeuchi, A., Hashizume, M., Kitamura, K., Kano, M., 2014. A highly sensitive fluorescent indicator dye for calcium imaging of neural activity in vitro and in vivo. Eur. J. Neurosci. 39, 1720–1728. https://doi.org/10.1111/ejn.12476.
Tawa, E.A., Hall, S.D., Lohoff, F.W., 2016. Overview of the genetics of alcohol use disorder. Alcohol Alcohol 51, 507–514. https://doi.org/10.1093/alcalc/agw046.
Tuithof, M., ten Have, M., van den Brink, W., Vollebergh, W., de Graaf, R., 2013. Predicting persistency of DSM-5 alcohol use disorder and examining drinking patterns of recently remitted individuals: a prospective general population study. Addiction 108, 2091–2099. https://doi.org/10.1111/add.12309.
Valentino, R.J., Bangasser, D., van Bockstaele, E.J., 2013. Sex-biased stress signaling: the corticotropin-releasing factor receptor as a model. Mol. Pharmacol. 83, 737–745. https://doi.org/10.1124/mol.112.083550.
Varodayan, F.P., Patel, R.R., Matzeu, A., Wolfe, S.A., Curley, D.E., Khom, S., Gandhi, P.J., Rodriguez, L., Bajo, M., D'Ambrosio, S., Sun, H., Kerr, T.M., Gonzales, R.A., Leggio, L., Natividad, L.A., Haass-Koffler, C.L., Martin-Fardon, R., Roberto, M., 2022. The amygdala noradrenergic system is compromised with alcohol use disorder. Biol. Psychiatr. 91, 1008–1018. https://doi.org/10.1016/j.biopsych.2022.02.006.
Vazey, E.M., den Hartog, C.R., Moorman, D.E., 2018. Central Noradrenergic Interactions with Alcohol and Regulation of Alcohol-Related Behaviors, pp. 239–260. https://doi.org/10.1007/164_2018_108.
Vendruscolo, L.F., Barbier, E., Schlosburg, J.E., Misra, K.K., Whitfield, T.W., Logrip, M.L., Rivier, C., Repunte-Canonigo, V., Zorrilla, E.P., Sanna, P.P., Heilig, M., Koob, G.F., 2012. Corticosteroid-dependent plasticity mediates compulsive alcohol drinking in rats. J. Neurosci. 32, 7563–7571. https://doi.org/10.1523/JNEUROSCI.0069-12.2012.
Villavicencio-Tejo, F., Flores-Bastías, O., Marambio-Ruiz, L., Pérez-Reytor, D., Karahanian, E., 2021. Fenofibrate (a PPAR-α agonist) administered during ethanol withdrawal reverts ethanol-induced astrogliosis and restores the levels of glutamate transporter in ethanol-administered adolescent rats. Front. Pharmacol. 12.
Wemm, S.E., Larkin, C., Hermes, G., Tennen, H., Sinha, R., 2019. A day-by-day prospective analysis of stress, craving and risk of next day alcohol intake during alcohol use disorder treatment. Drug Alcohol Depend. 204, 107569 https://doi.org/10.1016/j.drugalcdep.2019.107569.
Wilcox, C.E., Tonigan, J.S., Bogenschutz, M.P., Clifford, J., Bigelow, R., Simpson, T., 2018. A randomized, placebo-controlled, clinical trial of prazosin for the treatment of alcohol use disorder. J. Addiction Med. 12, 339–345. https://doi.org/10.1097/ADM.0000000000000413.
Wu, X., Yang, Xiangyu, Song, L., Wang, Yang, Li, Y., Liu, Y., Yang, Xiaowei, Wang, Yijun, Pei, W., Li, W., 2021. A modified miniscope system for simultaneous electrophysiology and calcium imaging in vivo. Front. Integr. Neurosci. 15, 682019 https://doi.org/10.3389/fnint.2021.682019.
Yamashita, A., Yoshioka, S., 2019. In: Preedy, V.R.B. (Ed.), Chapter 40 - Relapse Risks in Patients with Alcohol Use Disorders. Academic Press, pp. 383–390. https://doi.org/10.1016/B978-0-12-813125-1.00040-4.
Yang, W., Yuste, R., 2017. In vivo imaging of neural activity. Nat. Methods 14, 349–359. https://doi.org/10.1038/nmeth.4230.
Zelikowsky, M., Hersman, S., Chawla, M.K., Barnes, C.A., Fanselow, M.S., 2014. Neuronal ensembles in amygdala, Hippocampus, and prefrontal cortex track differential components of contextual fear. J. Neurosci. 34, 8462–8466. https://doi.org/10.1523/JNEUROSCI.3624-13.2014.
Zhao, Z., Kim, S.C., Jiao, Y., Wang, Y., Lee, B.H., Kim, H.Y., Lee, C.W., Yang, C.H., Zhao, R., 2021. Solitary nitric oxide signaling mediates mild stress-induced anxiety and norepinephrine release in the bed nucleus of the stria terminalis during protracted ethanol withdrawal. Behav. Neurol. 2021, 1–12. https://doi.org/10.1155/2021/2149371.